THE JOURNAL OF PHYSICAL CHEMISTRY C

ARTICLE

pubs.acs.org/JPCC

# Molecular Insight Into the Energy Levels at the Organic Donor/Acceptor Interface: A Quantum Mechanics/Molecular Mechanics Study

Shane R. Yost, Lee-Ping Wang, and Troy Van Voorhis*

Department of Chemistry, Massachusetts Institute of Technology, Cambridge, Massachusetts 02139-4307, United States

Supporting Information

**ABSTRACT:** We present an investigation of the band levels and charge transfer (CT) states at the interface between two organic semiconductors, metal-free phthalocyanine ($H_2Pc$) and 3,4,9,10-perylenetetracarboxylic bisbenzimidazole (PTCBI), using a combined quantum mechanics/molecular mechanics (QM/MM) technique. Near the organic−organic interface, significant changes from the bulk, as large as 0.2 eV, are found in the excited state energies, ionization potentials, and electron affinities, due to differences in molecular packing and polarizabilities of the two molecules. The changes in the ionization potential and electron affinity cause the CT states at the interface to be on average higher in energy than fully separated charges in the bulk materials despite having a typical local binding energy of 0.15 eV. Furthermore, we find that thermal fluctuations can induce variations of up to 0.1 eV in the CT binding energy. These results suggest that it is possible for bound interfacial CT states to dissociate in a barrierless fashion without involving "hot" CT states. This observation has direct relevance to the design of more efficient organic photovoltaics.

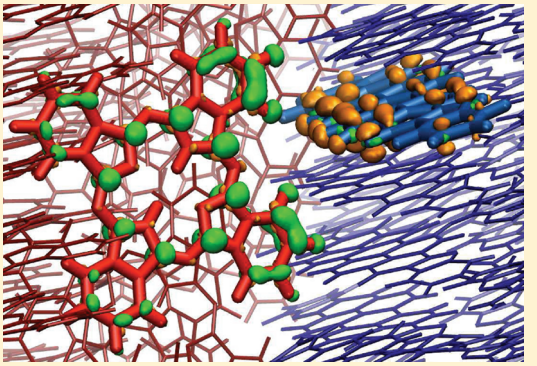

## INTRODUCTION

Organic semiconductors (OSCs) consist of $\pi$-conjugated organic molecules that typically absorb/emit in the UV−visible and can transport holes/electrons.[1] These properties make OSCs effective compounds for use in devices such as organic light emitting diodes (OLEDs)[2,3] and organic photovoltaics (OPVs).[4,5] These devices derive their functionality from at least one interface between two OSC materials; this is where excitons are converted into charge transfer (CT) states or vice versa, caused by the offset in the HOMO and LUMO energy levels of the different molecules.[6] The electrostatic environment near this interface can be dramatically different from the bulk due to the different packing and polarization of the two molecular layers,[7] leading to effects like interface dipoles[8,9] and band bending.[10] These phenomena can have a profound influence on carrier generation and loss mechanisms in OPVs and OLEDs, but the underlying physical chemistry is as of yet poorly understood.

The main intermolecular interaction in OSC devices is the weak van der Waals force, which allows for larger thermal fluctuations and greater disorder, especially at an interface. These effects can lead to Anderson localization[11] of carrier states on a few molecules or even a single molecule. On the basis of this localization model, one expects a combined quantum mechanics/molecular mechanics (QM/MM)[12] scheme to give a faithful description of the organic−organic interface. Indeed, we have successfully used QM/MM to model a crystalline OSC ($Alq_3$),[13] yielding quantitative predictions for both transport and optical properties. In this study, we use the QM/MM framework to gain further insight into the energetics at the organic−organic interface.

Numerous experimental studies have found general effects such as fast CT separation and the formation of an interface dipole in a variety of molecular interfaces.[14,15] Hence, in our study we simulate the interface between two molecules that have been individually well characterized: metal-free phthalocyanine ($H_2Pc$) and 3,4,9,10-perylenetetracarboxylic bisbenzimidazole (PTCBI), structures in Figure 1. Both are planar organic molecules with extensive $\pi$-conjugation, and the combination of these materials is experimentally known to form a functional photovoltaic device.[16] PTCBI has been studied in many different devices with phthalocyanines and other OSCs;[17−20] its high electron affinity and broad absorption in the visible region make it a widely used acceptor material. Phthalocyanine molecules are widely used as a small molecule donor material, and there exists a gamut of studies on $H_2Pc$ ranging from the gas phase[21] to the solid phase.[22,23]

Using the QM/MM model, we obtained an atomistic picture of the $H_2Pc$/PTCBI interface which reproduces the necessary energy level orderings for a functioning OPV device. Our calculated excitation energies reveal that thermal broadening

**Received:** April 11, 2011
**Revised:** June 6, 2011
**Published:** June 06, 2011

accounts for only a fraction of the absorption width. Near the interface we find shifted values in the IP and EA, showing that band bending effects at the interface *must* be included to accurately estimate the binding energies of the interfacial CT states. Further, the CT binding energy shows sensitivity to the relative molecular orientations and thermal fluctuations, highlighting the influence of disorder on the energy landscape. Importantly, the combination of band bending effects and fluctuations in CT binding energies makes it possible for relaxed CT states to dissociate into free carriers *with no barrier*. This finding improves our understanding of exciton dissocation and carrier generation mechanisms in OPVs, which is a subject of much current interest.[24−26] Our results show that charge separation efficiencies can be improved by decreasing the amount of charge solvation at the interface, which can be realized by designing an interface with relatively sparse packing.

The rest of this paper is organized as follows. We first introduce our computational technique, including QM and MM methods used. Next, we present the results of our calculations on pure materials and discuss their accuracy in comparison to experimental data. We then turn to the the organic−organic interface and discuss its effects on excitons and free carriers, in comparison to the bulk materials; here we also perform a detailed investigation of the interfacial CT state. Finally, we summarize the implications of our results for OPVs and discuss the insight gained on the carrier generation mechanism.

## COMPUTATIONAL DETAILS

Our study can be divided into (1) calculations performed on bulk $H_2Pc$ and PTCBI systems and (2) calculations performed on the $H_2Pc$/PTCBI interface; this allows us to benchmark our calculations by comparing to experimental measurements on single crystals and also examine effects of the interface by comparing bulk and interface calculations. Each study began with a pure NVT MM dynamics simulation, where the simulation cell contained several hundred molecules that are treated classically (Figure 2 left). Our simulation cells were ideal crystals in the sense that there were no site defects, and the interface was constructed from perfectly cleaved crystal faces. Several snapshots were harvested from this MM dynamics trajectory. In a given snapshot, a select few molecules were chosen to be treated quantum mechanically while interacting with the MM environment (Figure 2 middle). QM/MM single-point calculations were then performed to obtain the relevant material properties and repeated over many snapshots to obtain ensemble averaged values (Figure 2 right). We refer the reader to our previous work[13] and the Supporting Information for simulation details including the form of the MM force field and the method used to construct the parameters.

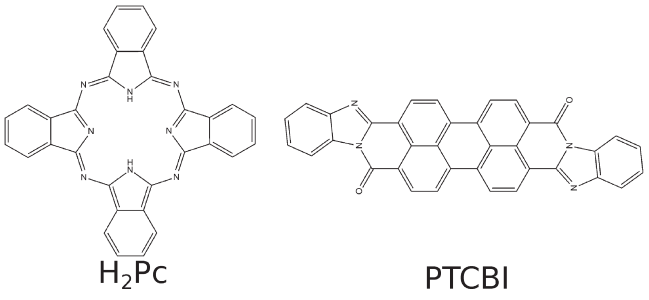


**Figure 1.** Molecular structures of $H_2Pc$ and PTCBI.

**Interface Structure.** For construction of the MM systems, we started with a pure $14 \times 7 \times 5$ ($3 \times 14 \times 5$) supercell of the experimental cyrstal structure for a total of 490 (420) PTCBI ($H_2Pc$) molecules. The $H_2Pc$/PTCBI interface was constructed by aligning the (001) and (010) crystal faces of the $H_2Pc$ and PTCBI supercells along $\hat{z}$; periodic boundary conditions were applied along $\hat{x}$ and $\hat{y}$ (i.e., perpendicular to the interface), and the system was relaxed under constant pressure (1 bar and 300 K) for 1 ns. All three systems were evolved under NVT dynamics for 5 ns at 300 K. The final 4 ns of the constant-volume dynamics was sampled at 40 ps intervals to obtain 100 snapshots for QM/MM calculations; the 40 ps time interval was chosen to minimize correlations between snapshots.

**Density Functional Calculations.** All of the QM/MM calculations were done using the CHARMM[27]−Q-Chem[28] interface,[29] and all pure MM calculations were run in Gromacs 4.0.[30] All quantum calculations were performed with Q-Chem 3.2 using the PBE0 functional and 6-31G* basis set. All of the singlet excited state calculations used linear-response time-dependent density functional theory (TDDFT)[31] on one molecule. The charge transfer states were obtained using constrained DFT[32] on two molecules with an extra electron placed on PTCBI and one electron removed from $H_2Pc$. The PBE0 functional was chosen because it offered the best compromise between accurate prediction of the singlet energy and the band offset, as the singlet energies increased and the band offset decreased with respect to the fraction of exact Hartree−Fock exchange for various functionals tested (PBE0 contains 25% exact exchange).

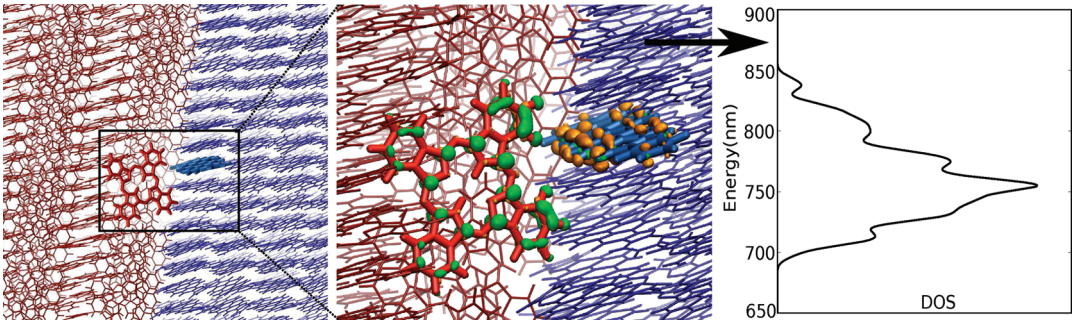


**Figure 2.** Illustration of the QM/MM method. Left: Disordered cell of the $H_2Pc$/PTCBI system described by MM. Center: Selection of a $H_2Pc$ and PTCBI pair at the interface for calculation of the CT state energy. Right: Density of states plot obtained by repeating the calculation over different snapshots of a MM trajectory.

**Table 1. Calculated Transport Properties for $H_2Pc$ and PTCBI[a]**

| material | IP | EA | TG | band offset |
|---|---|---|---|---|
| $H_2Pc$ | 4.74 (5.2) | 2.43 (3.0) | 2.31 (2.2) | 1.54 (1.6) |
| PTCBI | 5.53 (6.2) | 3.20 (3.6) | 2.33 (2.6) | |

[a] Experimental values, taken from refs 46, 47, and 48 are given in parentheses. All values are reported in eV; computed values have a statistical uncertainty of *le* 0.07 eV.

## RESULTS AND DISCUSSION

**Bulk Materials.** We started by computing the band offset and Frenkel exciton energies of bulk $H_2Pc$ and PTCBI, given in Table 1. To obtain the IP and EA values, we collected data from three different monomers in 20 distinct snapshots; the transport gap (TG) for a single material was given by $E_{IP} - E_{EA}$ and the bulk band offset by $E_{offset} = E_{IP}^{H_2Pc} - E_{EA}^{PTCBI}$. Here we note that the TGs and band offset, the more critical quantities for device performance, are in good agreement with experimental values despite larger errors in the IPs and EAs themselves. This is because there are roughly equal shifts in the IP and EA when increasing the basis set (+0.2 eV with 6-311G*) and when placing a molecule in the electrostatic environment of the crystal (−0.3 eV). A more detailed look into the basis set convergence can be found in the Supporting Information.

Turning our attention to optical properties, we note that most OSC materials have a broad absorption in the solid phase due to many different effects such as heterogeneous broadening, coupling between excited states (Davydov splitting) and vibronic transitions. The inclusion of all of these effects is beyond the scope of this study, and here we focus on heterogeneous broadening only. We computed the lowest few singlet excited state energies and their oscillator strengths for 15 different molecules over 50 snapshots. We then plotted each state as a Gaussian weighted by its oscillator strength to get absorption spectra, which are plotted with the experimental spectra[33] in Figure 3. Both of the absorption features are in roughly the right spectral region, but we note that with only heterogeneous broadening the calculated lineshapes are not nearly as broad as the experimental results. It thus appears that Franck−Condon (FC) and/or Herzberg−Teller (HT) effects play a significant role in determining OSC absorption spectra, even in disordered environments.[34,35]

Looking at PTCBI in particular, our calculated spectrum is also missing a peak at around 660 nm. This peak is also absent with the higher-accuracy RI-CC2[36] method in Turbomole[37] with the larger TZVP basis, which predicts only one bright peak at ∼525 nm. We suspect the missing peak is an HT effect; specifically, with either PBE0 or RI-CC2, there is a "dark" state in the 600−700 nm range with an oscillator strength that is essentially zero. This creates an ideal situation for the HT effect where the dark exciton could borrow intensity from the bright state via vibronic coupling.[35] For $H_2Pc$ our calculations underestimate the splitting of the *Qx* and *Qy* bands (given in order of increasing energy). This reflects a shortcoming of TDDFT for individual $H_2Pc$ molecules, as the splitting of the two peaks and their relative heights arise primarily from the symmetry lowering brought about by the two hydrogens in the inner ring, with the *Qx* (*Qy*) transition dipole parallel (perpendicular) to the line connecting the two inner hydrogens.

To better picture these excitons, the attachment−detachment plots[38] of the lowest singlet excited state for both molecules are shown alongside their spectra in Figure 3. Both of the molecules have a strong transition dipole in the molecular plane; for PTCBI, it points along the long molecular axis. The strength and alignment of the transition dipole moments suggest that exciton−exciton coupling in the solid phase could also have a significant effect on the lineshapes[39,40] of these crystalline materials, although we expect such effects to diminish in more realistic, disordered systems. In summary, our current implementation of the QM/MM model can reproduce the band offset accurately and obtain a qualitative picture of the excitonic levels, but obtaining a more accurate spectrum would require combining all of the above physical effects with the heterogeneous broadening presented here.

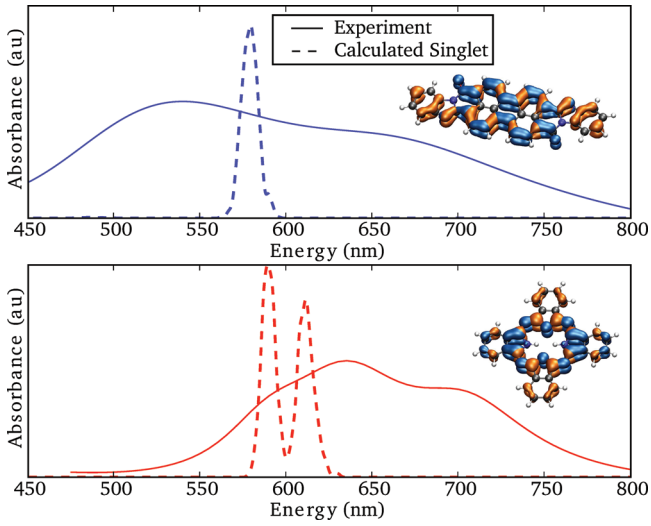


**Figure 3.** Calculated absorption spectrum (dashed) and experimental spectrum (solid) of PTCBI (top, blue) and $H_2Pc$ (bottom, red). The calculated spectra contain 750 calculated energies sampled from 15 molcules each over 50 snapshots, each given a Gaussian distribution with width of 1.7 nm. The inserted molecules show the attachment/detachment (blue/orange) densities of the lowest excited state of PTCBI and $H_2Pc$.

**Organic−Organic Interface.** Next, we examine the absorption spectra in the interface system. The absorption spectra at the interface are plotted in Figure 4 along with the bulk spectra reproduced from Figure 3. The absorption curve of PTCBI is red-shifted, and the splitting in $H_2Pc$ is reduced for excitons closer to the interface; these changes indicate a shift toward gas-phase values, likely due to the less dense packing at the interface. In contrast, the interface has a negligible effect on molecules located ≥2 nm (1−2 molecules) away; this agrees with our expectation that the highly localized exciton is not very susceptible to electrostatic changes.

The CT state, on the other hand, is more susceptible to changes in the electrostatic environment and is correspondingly more sensitive to the interface. We sampled five crystallographically distinct nearest-neighbor CT pairs at the interface using over 20 snapshots and plotted their density of states alongside the absorption spectra in Figure 5. By comparing the energy levels, we see that a singlet exciton in either material is able to transfer its energy into an interfacial CT state, which can then separate into isolated charges; thus, our calculations correctly reproduce the experimental observation that PTCBI/$H_2Pc$ forms a functional photovoltaic device.[16] Not surprisingly, the CT states have a broader energy distribution (fwhm ∼220 meV) than excitonic states; this is in part due to the distribution of CT

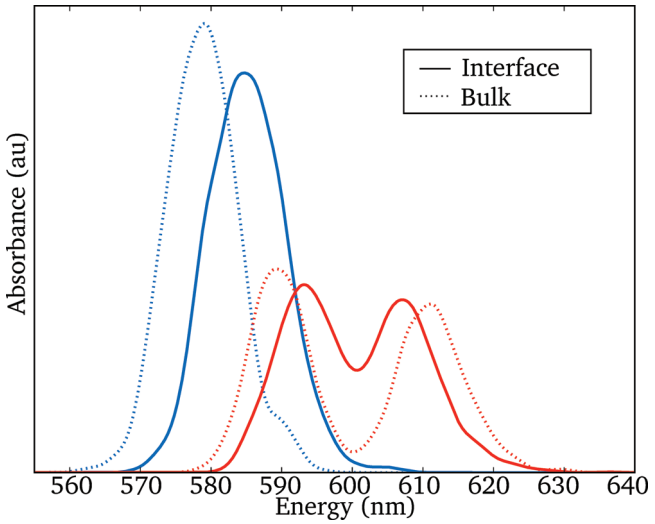


**Figure 4.** Calculated absorption spectrum of $H_2Pc$ (red) and PTCBI (blue) at the organic−organic interface (solid) and in the bulk (dashed). Each curve was constructed from 750 different values sampled from 15 molecules each over 50 snapshots and given a Gaussian distribution with width 1.7 nm.

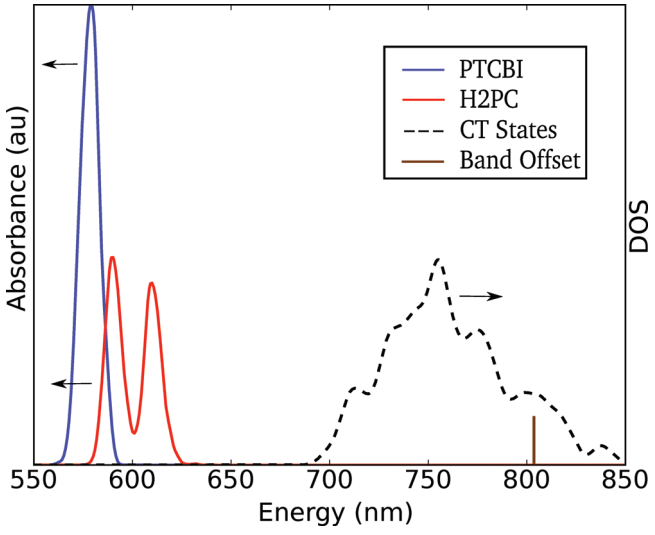


**Figure 5.** Full calculated spectra of all relevant energy states: bulk absorption (left axis) of $H_2Pc$ (red) and PTCBI (blue), CT density of states (black, right axis), and the location of the average bulk band offset (brown). Each data point is given a Gaussian distribution with a width of 1.7 nm.

pairs, most notably the variation in the donor−acceptor distance between different pairs. By contrast, the dynamic fluctuations of the CT energy for a given pair are much smaller (fwhm ∼60 meV).

We performed further analysis on the distance dependence of the CT binding energy (BE, given by $E_{BE} = (E_{IP}^{H_2Pc} - E_{EA}^{PTCBI}) - E_{CT}$). Using the procedure provided in ref 41, we fit the inverse of the BE to a linear combination of intermolecular distances; our results are shown in Figure 6. We chose to use a linear combination of intermolecular distances for the coordinate in Figure 6 to filter out the effects of relative molecular orientation as much as possible; further details of this coordinate can be

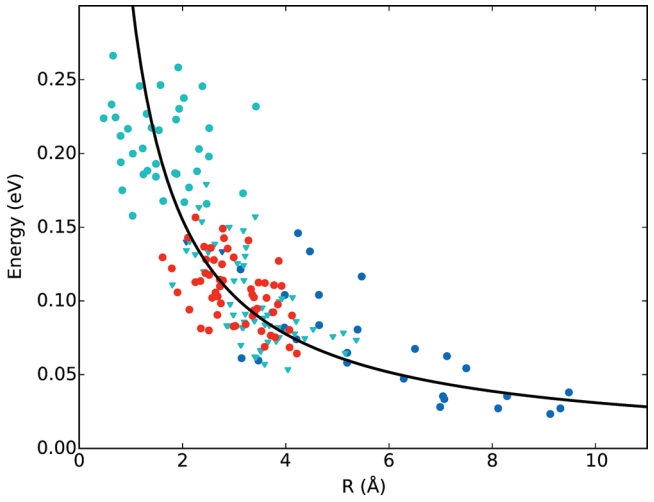


**Figure 6.** Plot of the distance dependence of the PTCBI/$H_2Pc$ CT state binding energies. The coordinate $R$ is a linear combination of intermolecular distances. Each different color/shape combination represents distinct dimer pairs in the simulation cell.

found in the Supporting Information. The BE has a clear $R^{-1}$ decay as a function of distance, arising from the Coulomb interaction between the electron on the acceptor and the hole on the donor; however, this trend was not observed when center-of-mass or closest contact distances were used, highlighting the important orientational dependence for these planar molecules. The average BE for the closest pairs is 0.2 eV, while averaging over all of the nearest neighbor pairs yields a BE of 0.15 eV for the CT states. The overall fit is good, with a correlation of 0.85 between the data and $R^{-1}$; there is also a clear scatter of 0.1 eV on top of the Coulombic decay which we attribute to thermal fluctuations. From moment to moment, the CT energy of a given dimer will fluctuate by a few kT. Thus, at any instant there can easily be a more distant CT pair that has a lower energy than a compact pair due to random fluctuations in molecular orientation. These variations are expected to aid the initial charge separation at the organic−organic interface.

Perhaps surprisingly, the average energy of the CT states (1.6 eV) is higher than the bulk band offset (1.5 eV), giving an apparent CT binding energy of ≈−0.1 eV; that is to say, the CT states seem to be unbound! We found that this can be explained by the significant contribution of interface effects to the band offset. In Figure 7 we plot the IP and EA of $H_2Pc$/PTCBI vs the distance from the interface, and each point corresponds to an average over four monomers each using 20 snapshots. The EA of PTCBI (IP of $H_2Pc$) decreases (increases) as one moves toward the interface by 0.1 (0.15) eV, such that the band offset at the interface is 0.25 eV larger than the bulk value and giving an average CT binding energy of ≈0.15 eV. Thus, the CT states are *locally* bound; the energy of the electron−hole pair at the interface is more stable than a single electron plus a single hole at the same site. At the same time, the CT states are *globally* unbound; the electron and hole gain energy by migrating away from the interface.

The "gap bending" effect at the OSC donor−acceptor interface has been previously calculated in different systems and with different models.[8,42,43] In those cases, the effect was caused by an interfacial dipole that shifted the electron and hole levels asymmetrically. Our calculations did not find a significant dipole at the $H_2Pc$/PTCBI interface; instead, the gap bending appears

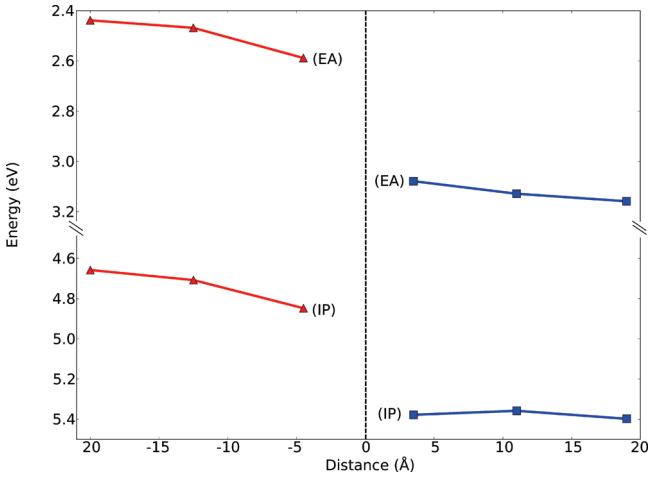


**Figure 7.** Plot of the average IP and EA of $H_2Pc$ (red) and PTCBI (blue) crystal planes as a function of their distance from the interface. Each point has a standard deviation of about 50 meV.

to be due to differences in the polarizability and crystal packing. The interface has a stabilizing (destabilizing) effect on carriers in $H_2Pc$ (PTCBI) because PTCBI has a higher dielectric constant than $H_2Pc$, and the relatively sparse packing introduces an overall destabilizing effect; our QM/MM simulations with a polarizable MM model were uniquely able to capture these effects.[13]

There is much discussion in the literature on understanding the origins of the high internal quantum efficiency in OPVs and why the separation of a CT state appears to be essentially barrierless.[44] One prominent view is that the excess energy from exciton dissociation creates a "hot" CT state with sufficient kinetic energy to break free of the binding energy before thermal relaxation takes place.[24,25] On the other hand, there is also evidence that thermally relaxed CT states are separating into free charges.[26,45] Our work indicates the latter model to be more accurate and suggests that thermally relaxed CT states can break up easily due to competition between the decreased dielectric screening at the interface and the Coulomb attraction, the first increasing and the second decreasing the CT energy. For our current $H_2Pc$/PTCBI model system, the decrease in dielectric screening is larger than the Coulomb attraction, and thus there is little to no energy barrier for CT separation. Future studies spanning a broad range of molecules and interfaces would be useful for testing the generality of these results.

## CONCLUSION

In this study, we used a QM/MM model to investigate the $H_2Pc$/PTCBI donor−acceptor interface and obtained thermal distributions of the exciton, IP, EA, and CT energies. We obtained an accurate prediction of the band offset for this interface system and a qualitative description of the excitonic states. We also find a strong dependence of the BE on the relative orientation of the molecules forming the CT pair. One route to decrease charge recombination is to lower the CT binding energy by maximizing the edge-to-edge stacking at the donor−acceptor interface and minimizing the cofacial stacking. We addressed two effects on the CT state energy that depend on proximity to the interface: the electrostatic changes at the interface cause the band offset to increase by 0.25 eV, and the CT binding energy is strongest at the interface with a typical value of 0.15 eV. The competition between two effects creates a situation where thermally relaxed CT states at the interface can easily separate into free carriers. In our model system, charge separation is downhill by about 0.1 eV.

The current set of calculations has helped to clarify the molecular processes at an organic−organic interface, but there are a number of effects that still need to be included in the calculations. First, to get a more accurate absorption spectrum, the Franck−Condon factors, Herzberg−Teller corrections, and exciton coupling should be included; any of these effects can shift the peaks as well as significantly broaden them. Second, the effect of vacancy and substitutional defects on the performance of OSC devices needs to be studied since realistic interfaces in thin films are less ideal than the one presented in this study. Finally, it would be fruitful to extend this study to different OSC molecules, to aid in our understanding of how the interface affects the band offset in a variety of situations.

## ASSOCIATED CONTENT

**Supporting Information.** All of the MM paramaters and unit cells used, as well as the "course-grained" model used to obtain the distance dependence of the CT binding energy. This material is available free of charge via the Internet at http://pubs.acs.org.

## AUTHOR INFORMATION

**Corresponding Author**
*E-mail: tvan@mit.edu.

## ACKNOWLEDGMENT

T.V. gratefully acknowledges fellowships from the Packard Foundation and the Sloan Foundation. The work on optical properties, energy level alignment, and CT formation was supported by the U.S. Department of Energy under DE-FG02-07ER46474. L.P.W.'s work on the construction of the MM parameters and crystal structures thanks ENI SpA as part of the Solar Frontier Research Program.

## REFERENCES

(1) Pope, M.; Swenberg, C. E. *Electronic Processes in Organic Crystals and Polymers*; Oxford University Press: New York, 1999.
(2) Friend, R.; Gymer, R.; Holmes, A.; Burroughes, J.; Marks, R.; Taliani, C.; Bradley, D.; Dos Santos, D.; Brédas, J.; Logdlund, M.; Salaneck, W. *Nature* **1999**, *397*, 121–128.
(3) Hung, L.; Chen, C. *Mater. Sci. Eng. R* **2002**, *39*, 143–222.
(4) Forrest, S. R. *Nature* **2004**, *428*, 911–918.
(5) Guenes, S.; Neugebauer, H.; Sariciftci, N. S. *Chem. Rev.* **2007**, *107*, 1324–1338.
(6) Brédas, J.-L.; Norton, J. E.; Cornil, J.; Coropceanu, V. *Acc. Chem. Res.* **2009**, *42*, 1691–1699.
(7) Armstrong, N. R.; Wang, W.; Alloway, D. M.; Placencia, D.; Ratcliff, E.; Brumbach, M. *Macromol. Rapid Commun.* **2009**, *30*, 717–731.
(8) Linares, M.; Beljonne, D.; Cornil, J.; Lancaster, K.; Brédas, J.-L.; Verlaak, S.; Mityashin, A.; Heremans, P.; Fuchs, A.; Lennartz, C.; Ide, J.; Mereau, R.; Aurel, P.; Ducasse, L.; Castet, F. *J. Phys. Chem. C* **2010**, *114*, 3215–3224.
(9) Arkhipov, V.; Heremans, P.; Bassler, H. *Appl. Phys. Lett.* **2003**, *82*, 4605–4607.
(10) Ishii, H.; Sugiyama, K.; Ito, E.; Seki, K. *Adv. Mater.* **1999**, *11*, 605.
(11) Anderson, P. *Phys. Rev.* **1958**, *109*, 1492–1505.

(12) Åqvist, J.; Warshel, A. *Chem. Rev.* **1993**, *93*, 2523–2544.
(13) Difley, S.; Wang, L.-P.; Yeganeh, S.; Yost, S. R.; Van Voorhis, T. *Acc. Chem. Res.* **2010**, *43*, 995–1004.
(14) Molodtsova, O.; Schwieger, T.; Knupfer, M. *Appl. Surf. Sci.* **2005**, *252*, 143–147.
(15) Zhang, F.; Vollmer, A.; Zhang, J.; Xu, Z.; Rabe, J.; Koch, N. *Org. Electron.* **2007**, *8*, 606–614.
(16) Abe, T.; Miyakushi, S.; Nagai, K.; Norimatsu, T. *Phys. Chem. Chem. Phys.* **2008**, *10*, 1562–1568.
(17) Hiromitsu, I.; Murakami, Y.; Ito, T. *J. Appl. Phys.* **2003**, *94*, 2434–2439.
(18) Triyana, K.; Yasuda, T.; Fujita, K.; Tsutsui, T. *Thin Solid Films* **2005**, *477*, 198–202.
(19) Forrest, S.; Leu, L.; So, F.; Yoon, W. *J. Appl. Phys.* **1989**, *66*, 5908–5914.
(20) Haskal, E.; Shen, Z.; Burrows, P.; Forrest, S. *Phys. Rev. B* **1995**, *51*, 4449–4462.
(21) Eastwood, D.; Edwards, L.; Gouterma, M.; Steinfel, J. *J. Mol. Spectrosc.* **1966**, *20*, 381.
(22) Dozova, N.; Murray, C.; McCaffrey, J. G.; Shafizadeh, N.; Crepin, C. *Phys. Chem. Chem. Phys.* **2008**, *10*, 2167–2174.
(23) Mizuguchi, J.; Matsumoto, S. *J. Phys. Chem. A* **1999**, *103*, 614–616.
(24) Clarke, T. M.; Ballantyne, A. M.; Nelson, J.; Bradley, D. D. C.; Durrant, J. R. *Adv. Funct. Mater.* **2008**, *18*, 4029–4035.
(25) Zhu, X. Y.; Yang, Q.; Muntwiler, M. *Acc. Chem. Res.* **2009**, *42*, 1779–1787.
(26) Lee, J.; Vandewal, K.; Yost, S. R.; Bahlke, M. E.; Goris, L.; Baldo, M. A.; Manca, J. V.; Van Voorhis, T. *J. Am. Chem. Soc.* **2010**, *132*, 11878–11880.
(27) Brooks, B. R.; Bruccoleri, R. E.; Olafson, B. D.; States, D. J.; Swaminathan, S.; Karplus, M. *J. Comput. Chem.* **1983**, *4*, 187–217.
(28) Shao, Y.; et al. *Phys. Chem. Chem. Phys.* **2006**, *8*, 3172–3191.
(29) Woodcock, H. L., III; Hodošček, M.; Gilbert, A. T. B.; Gill, P. M. W.; Shaefer, H. F., III; Brooks, B. R. *J. Comput. Chem.* **2007**, *28*, 1485–1502.
(30) Hess, B.; Kutzner, C.; van der Spoel, D.; Lindahl, E. *J. Chem. Theory Comput.* **2008**, *4*, 435–447.
(31) Dreuw, A.; Head-Gordon, M. *Chem. Rev.* **2005**, *105*, 4009–4037.
(32) Wu, Q.; Van Voorhis, T. *Phys. Rev. A* **2005**, *72*, 024502.
(33) Lee, J.; Baldo, M. A. personal communication.
(34) Santoro, F.; Lami, A.; Improta, R.; Barone, V. *J. Chem. Phys.* **2007**, *126*, 184102.
(35) Santoro, F.; Lami, A.; Improta, R.; Bloino, J.; Barone, V. *J. Chem. Phys.* **2008**, *128*, 224311.
(36) Hattig, C.; Kohn, A. *J. Chem. Phys.* **2002**, *117*, 6939–6951.
(37) Ahlrichs, R.; Bar, M.; Haser, M.; Horn, H.; Kolmel, C. *Chem. Phys. Lett.* **1989**, *162*, 165–169.
(38) Head-Gordon, M.; Grana, A. M.; Maurice, D.; White, C. A. *J. Phys. Chem.* **1995**, *99*, 14261–14270.
(39) Spano, F. C. *Annu. Rev. Phys. Chem.* **2006**, *57*, 217–243.
(40) Cornil, J.; dos Santos, D. A.; Crispin, X.; Silbey, R.; Brédas, J. L. *J. Am. Chem. Soc.* **1998**, *120*, 1289–1299.
(41) Mahata, K.; Mahata, P. Maximizing Correlation for Supervised Classification. *Proceedings of the 2007 15th International Conference on Digital Signal Processing*, 2007; pp 107−110.
(42) Vazquez, H.; Gao, W.; Flores, F.; Kahn, A. *Phys. Rev. B* **2005**, *71*, 041306.
(43) Verlaak, S.; Beljonne, D.; Cheyns, D.; Rolin, C.; Linares, M.; Castet, F.; Cornil, J.; Heremans, P. *Adv. Funct. Mater.* **2009**, *19*, 3809–3814.
(44) Pensack, R. D.; Asbury, J. B. *J. Am. Chem. Soc.* **2009**, *131*, 15986.
(45) Zhou, Y.; Tvingstedt, K.; Zhang, F.; Du, C.; Ni, W.-X.; Andersson, M. R.; Inganas, O. *Adv. Funct. Mater.* **2009**, *19*, 3293–3299.
(46) Pope, M. *J. Chem. Phys.* **1962**, *36*, 2810.
(47) Zahn, D.; Gavrila, G.; Gorgoi, M. *Chem. Phys.* **2006**, *325*, 99–112.
(48) Rand, B. P.; Genoe, J.; Heremans, P.; Poortmans, J. *Prog. Photovoltaics Res. Appl.* **2007**, *15*, 659–676.